land

MDPI

Article

Grassland Ecological Dynamics Before and During Precipitation Seeding and Their Long-Term Climatic Drivers in Wuqia County, China: An Observational Comparison

Chao Guo [1,2], Batur Bake [1,2,*], Akida Salam [3], Alim Abbas [1,2], Adile Kurban [1], Xinyuan Zhang [1], Chen Cheng [4] and Zulian Zhang [5]

[1] College of Resources and Environmental Sciences, Xinjiang Agricultural University, Urumqi 830052, China
[2] Xinjiang Key Laboratory of Soil and Plant Ecological Processes, Urumqi 830052, China
[3] Meteorological Bureau of Kizilsu Kirgiz Autonomous Prefecture, Artux 845350, China
[4] Meteorological Bureau of the Tenth Division of Xinjiang Production and Construction Corps, Beitun 836099, China
[5] Xinjiang Uygur Autonomous Region Climate Center (Xinjiang Environmental Resources Remote Sensing Center), 327 Jianguo Road, Urumqi 830002, China
* Correspondence: baturbake@xjau.edu.cn

Abstract

Arid, high-elevation grasslands are sensitive to hydrothermal variability, highlighting the need to characterize their ecological dynamics and climatic drivers. Using multi-source remote sensing and meteorological data from Wuqia County, Xinjiang, China, we compared observed changes in growing-season normalized difference vegetation index (NDVI), fractional vegetation cover (FVC), net primary productivity (NPP), and the vegetation ecological quality index (VEQI) between the periods before (2018–2021) and during (2022–2025) precipitation seeding (PS) operations. Ridge regression was applied to assess the contributions of four climatic predictors to long-term NDVI trends during 2000–2025. The proportion of grassland exhibiting slight or greater NDVI improvement increased from 11.43% to 46.52% between the two periods, with improvements concentrated in northeastern Wuqia County. Differences in period-specific trend slopes were 1.4977 percentage points yr^{-1} for FVC, 2.0138 g C m^{-2} $season^{-1}$ yr^{-1} for NPP, and 4.7423 index points yr^{-1} for VEQI, with positive slope differences covering 80.48%, 85.82%, and 86.53% of the grassland area, respectively. The four-predictor long-term trend model assigned the largest mean relative contribution to temperature (55.47%), followed by potential evapotranspiration (18.35%), precipitation (13.72%), and solar radiation (12.46%). Positive modeled temperature contributions occurred across 97.62% of the grassland area. However, temporal cross-validation indicated limited predictive performance (mean $R^2 = -0.3986$), while bootstrap analysis revealed uncertainty in temperature's ranking (63.23% probability of ranking first). Although grassland ecological indicators exhibited higher estimated trend slopes during the PS operational period, these observational differences cannot be attributed independently to PS because of natural climatic variability, concurrent conservation measures, and limitations of the study design. These findings provide insights into grassland ecological dynamics and their modeled climatic associations in arid, high-elevation regions, without establishing the ecological effectiveness of PS.

Keywords: precipitation seeding; grassland ecological change; normalized difference vegetation index; ridge regression; climatic drivers

Check for updates

Academic Editor: Jane Southworth

Received: 17 October 2026
Revised: 13 November 2026
Accepted: 19 November 2026
Published: 27 November 2026

Copyright: © 2026 by the authors. Licensee MDPI, Basel, Switzerland. This article is an open access article distributed under the terms and conditions of the Creative Commons Attribution (CC BY) license.

1. Introduction

In arid mountainous regions, water availability and thermal conditions jointly regulate vegetation growth in high-elevation grasslands [1,2]. Located on the northeastern margin of the Pamir Plateau, Wuqia County in Xinjiang, China, is characterized by extensive mountain grasslands that are sensitive to variations in moisture and thermal conditions. Routine precipitation seeding (PS) operations were initiated in 2022, providing a temporal reference for examining grassland ecological changes before and during PS operations. As ecological conservation and restoration efforts expand, precipitation seeding is being considered as an additional means of increasing water availability, particularly in regions where water scarcity limits ecological recovery [3–5]. Accordingly, research has gradually expanded from evaluating precipitation enhancement effectiveness to assessing associated vegetation changes. For example, Ma et al. [6] found that precipitation in the precipitation seeding operational area of the Shiyang River Basin increased by an average of 20.8% relative to the reference level, accompanied by an increase in the proportion of vegetated land from 20.2% to 27.24%. Similarly, Gong et al. [7] reported an increase in the average vegetation ecological quality index across forest areas exposed to varying frequencies of precipitation seeding operations in the Greater Khingan Mountains compared with the period before implementation. However, existing studies have primarily focused on desert-oasis and forest ecosystems, whereas multi-indicator assessments of ecological changes in arid high-elevation grasslands before and during PS implementation remain limited.

Grassland ecological changes observed during the pre-PS and operational periods may also be influenced by natural climate variability and other human activities. Therefore, comparisons between pre- and post-implementation periods alone are insufficient to isolate the net ecological effects of precipitation seeding [4]. Examining long-term climatic influences on vegetation dynamics can provide important context for interpreting such changes. Zhang et al. [8] applied ridge regression to examine the relative importance of climatic variables in shaping net ecosystem productivity (NEP) in the Tianshan Mountains. Their analysis identified soil moisture as the dominant factor, followed by temperature, precipitation, and solar radiation. Although this work provides insights into the climatic controls on ecosystem productivity, the relative contributions of climatic factors to long-term trends in the normalized difference vegetation index (NDVI) across grasslands in Wuqia County, as well as their spatial variations, remain unclear.

Using 2022 as the dividing point for routine precipitation seeding (PS) operations, this study integrates multi-source remote sensing and meteorological data to compare observed grassland ecological changes in Wuqia County between the pre-PS (2018–2021) and PS operational (2022–2025) periods and quantify the relative contributions of climatic factors to long-term vegetation dynamics. Specifically, it addresses two research questions: (1) How did grassland ecological conditions and their spatial patterns differ between 2018–2021 and 2022–2025? (2) What were the contributions of individual climatic factors to long-term grassland NDVI changes during 2000–2025, and how did their relative importance differ across Wuqia County? Given the observational nature of the data, this study characterizes observed temporal differences between the two periods rather than isolating an independent net ecological effect of PS. The results revealed more favorable observed grassland ecological changes during the PS operational period and identified temperature as the leading modeled contributor to long-term NDVI trends, providing insights into vegetation dynamics and their climatic associations in arid, high-elevation regions.

2. Materials and Methods

2.1. Study Area

Wuqia County is located in southwestern Xinjiang, China, within the northwestern part of Kizilsu Kirgiz Autonomous Prefecture. Geographically, it occupies the eastern margin of the Pamir Plateau, where the southern Tianshan and Kunlun mountain ranges meet (73°40′–75°45′ E, 39°24′–40°17′ N). The county covers approximately 18,800 km^2, with elevations varying between 1760 and 6146 m (Figure 1). The climate is temperate and arid, with a mean annual temperature of 7.30 °C and an average annual precipitation of 172 mm. Annual sunshine duration reaches 2797.2 h, while the frost-free period lasts approximately 135 days. Complex topography and variations in moisture and thermal conditions contribute to pronounced spatial heterogeneity in vegetation distribution, which is dominated by desert vegetation and montane grasslands [9,10]. The main soil types include Aridisols, Cambisols, Solonchaks, Regosols, and Anthrosols [11]. The county is characterized by mountainous terrain, Gobi deserts, and barren landscapes, with desert grasslands covering approximately 10,667 km^2 [12]. Limited water availability, together with human disturbances such as grazing, makes local grassland ecosystems particularly vulnerable to environmental changes [12,13].

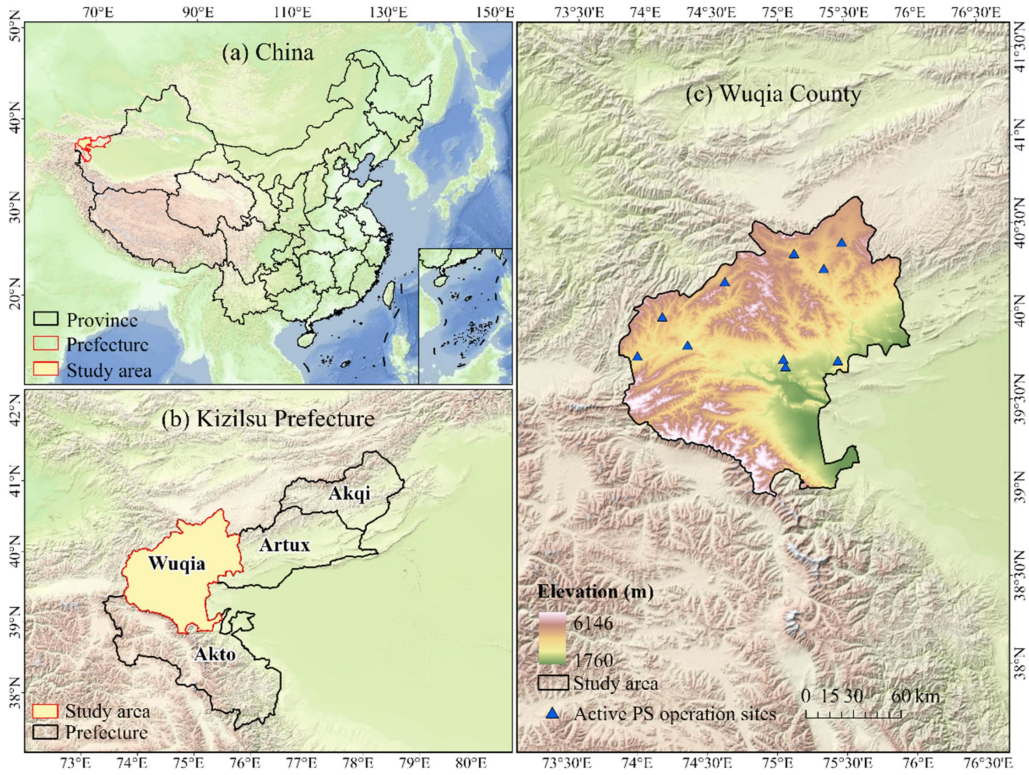


Figure 1. Geographic setting of Wuqia County, Xinjiang, China, and the distribution of active precipitation seeding (PS) operation sites. (**a**) Position of the study area within China; (**b**) administrative setting of Wuqia County within Kizilsu Kirgiz Autonomous Prefecture; and (**c**) topographic elevation and locations of active PS operation sites. Only the positions of the active operation sites are shown; these coordinates do not represent the spatial extent of precipitation enhancement or the areas affected by individual operations.

2.2. Data and Preprocessing

2.2.1. Satellite Data

The MODIS MOD13Q1 Vegetation Indices product (Collection 6.1), provided by the National Aeronautics and Space Administration (NASA), was used to derive NDVI for 2000–2025. The product provides observations at a spatial resolution of 250 m and a temporal resolution of 16 days. For long-term vegetation analysis, the NDVI time series was subjected to quality control, gap filling, and Savitzky–Golay (S-G) smoothing, followed by monthly maximum value compositing (MVC) to obtain growing-season NDVI [14]. For CASA-based NPP estimation during 2018–2025, monthly mean NDVI was calculated from quality-filtered observations. For long-term climatic attribution, valid 250 m NDVI pixels were aggregated to a 1 km grid using area-weighted means (Table 1).

Table 1. Data sources, product specifications, and preprocessing procedures used in this study.

Dataset	Product/Identifier	Period Used	Resolution	Original Units/Scale Factor	Main Processing
NDVI	MOD13Q1 V6.1 (https://earthdata.nasa.gov/)	2000–2025 (accessed on 6 January 2026)	250 m, 16-day	Dimensionless; ×0.0001	QA = 0 and 1 retained; QA = 2 and 3 excluded; linear interpolation of gaps ≤ 2 consecutive observations; S-G smoothing (window = 5, order = 2); monthly MVC and 4–9 mean for long-term analysis. For CASA, monthly mean of QA-filtered observations.
PRE	TPDC China 1 km Monthly Precipitation (https://data.tpdc.ac.cn/)	2000–2025 (accessed on 20 April 2026)	1 km, monthly	0.1 mm; ×0.1	Conversion to mm; monthly precipitation summed over 4–9 to obtain growing-season precipitation.
TMP	TPDC China 1 km Monthly Mean Temperature (https://data.tpdc.ac.cn/)	2000–2025 (accessed on 20 April 2026)	1 km, monthly	0.1 °C; ×0.1	Conversion to °C; 4–9 monthly mean.
PET	MOD16A2GF V6.1 (https://earthdata.nasa.gov/)	2000–2025 (accessed on 25 April 2026)	500 m, 8 day	kg m^{-2} per composite; ×0.1	Invalid-value screening; proportional allocation of 8-day totals to calendar months according to overlapping days; monthly totals calculated and averaged over 4–9.
Solar radiation	MCD18A1 V6.2 (https://earthdata.nasa.gov/)	2000–2025 (accessed on 27 April 2026)	1 km, daily	W m^{-2}; no scale factor	Eight three-hourly DSR bands; DSR_Quality flag screening; daily energy integration; monthly aggregation; 4–9 mean.
CASA meteorology	ERA5-Land Monthly Aggregated (ECMWF/ERA5_LAND/MONTHLY_AGGR)	2018–2025 (accessed on 8 January 2026)	0.1°, monthly	Variable-dependent	Temperature converted to °C; solar radiation converted to MJ m^{-2} and multiplied by 0.45 to derive PAR; absolute values of actual and potential evaporation used to calculate moisture stress.

Notes: QA = quality assurance; DSR = downward shortwave radiation. For long-term climatic attribution, valid 250 m NDVI pixels were aggregated to the common 1 km grid using an area-weighted mean.

The grassland mask was derived from a static vector layer of the 2020 grassland distribution in Wuqia County, compiled with reference to the Third National Land Survey. Grassland polygons were delineated through visual interpretation of high-resolution imagery, supported by field survey records, elevation data, and administrative boundaries, and were vectorized in ArcGIS10.8.1 (Esri, Redlands, CA, USA). All grassland categories were retained, while non-grassland areas were excluded. The same grassland mask was applied throughout the study. For the 250 m ecological analyses (2018–2025), 226,753 valid grassland pixels were retained, serving as the denominator for the area proportions reported in Table 2. For the 1 km climatic attribution analysis (2000–2025), the mask was rasterized to a 1 km grid in the CGCS2000 3° Gauss–Krüger projection, with pixels classified as grassland when grassland coverage exceeded 50%. After excluding pixels with incomplete records for the four climatic predictors, 9942 valid 1 km grassland pixels were retained for climatic attribution. The approximately 10,667 km^2 of grassland reported in Section 2.1 represents the literature-based county grassland area and is distinct from the effective analysis areas.

Table 2. Grassland area proportions across classes of changes in trend slopes for FVC, NPP, and VEQI between the pre-PS and PS periods in Wuqia County.

Trend Slope Change Class	FVC		NPP		VEQI	
	Trend (Percentage Points yr^{-1})	**Area Proportion (%)**	**Trend (g C m^{-2} Season^{-1} yr^{-1})**	**Area Proportion (%)**	**Trend (Index Points yr^{-1})**	**Area Proportion (%)**
Negative change	<0	19.52	<0	14.18	<0	13.47
Minimal improvement	0–1.00	21.87	0–0.50	14.40	0–1.00	4.61
Mild improvement	1.00–3.00	39.02	0.50–1.00	16.54	1.00–3.00	14.16
Moderate improvement	3.00–5.00	15.41	1.00–1.50	13.11	3.00–5.00	20.35
Large improvement	5.00–10.00	4.05	1.50–2.00	8.84	5.00–10.00	40.33
High improvement	>10.00	0.12	>2.00	32.93	>10.00	7.07
Total positive change	>0	80.48	>0	85.82	>0	86.53

Note: Area proportions were calculated relative to the valid grassland area used for the corresponding spatial trend analysis. For VEQI, the denominator comprised 226,753 valid grassland pixels. Minor discrepancies between the sum of individual classes and 100% are caused by rounding. These classes represent the magnitude of changes in trend slopes rather than statistical significance or changes in indicator levels. The class breaks were set at round values on each indicator's own scale (percentage points for FVC, g C m^{-2} season^{-1} for NPP, and index points for VEQI), so that classes are comparable within an indicator but not across indicators; they are descriptive bins and were not statistically optimized.

2.2.2. Meteorological Data

The climatic variables considered in this study comprised precipitation (PRE), mean air temperature (TMP), potential evapotranspiration (PET), and solar radiation (Solar). For long-term climatic attribution (2000–2025), monthly PRE and TMP were obtained from the China 1 km Monthly Precipitation and Monthly Mean Temperature datasets provided by the National Tibetan Plateau Data Center [15]. PET was derived from the MODIS MOD16A2GF V6.1 product, while solar radiation was obtained from the MODIS MCD18A1 V6.2 product. Growing-season precipitation was calculated as the sum of monthly values from April to September to represent cumulative water input, whereas TMP, PET, and Solar were averaged over the same period, with PET representing mean monthly atmo-

spheric evaporative demand rather than a seasonal water total; the two variables therefore describe different aspects of the hydrothermal environment and do not form a directly comparable seasonal water balance. For CASA-based NPP estimation during 2018–2025, meteorological inputs were obtained from the ERA5-Land Monthly Aggregated dataset (ECMWF/ERA5_LAND/MONTHLY_AGGR), including 2 m air temperature, downward surface solar radiation, actual evaporation, and potential evaporation. These variables were converted to the required units and used to calculate temperature and moisture stress factors and photosynthetically active radiation (PAR). The meteorological inputs were combined with MODIS-derived FPAR to estimate monthly NPP, which was subsequently accumulated over April to September to obtain growing-season NPP (Table 1).

2.2.3. Precipitation Seeding Operation Data

Precipitation seeding (PS) operation data were obtained from the Meteorological Bureau of Wuqia County and the Meteorological Bureau of Kizilsu Kirgiz Autonomous Prefecture. The dataset included the geographic coordinates of PS operation sites, operation types, and the number of operations during 2022–2025. During this period, a total of 12 PS operation sites were registered in Wuqia County, including 10 ground-based smoke generator sites and 2 rocket operation sites. Of these, 10 sites conducted PS operations, comprising 9 smoke generator sites and 1 rocket operation site. Between 2022 and 2025, 44 PS operations were conducted, comprising 33 smoke generator operations and 11 rocket operations (Table 3). The coordinates of these sites were used to map the geographic distribution of PS activities within the county.

Table 3. Statistics of PS operations in Wuqia County during 2022–2025.

Operation Period	Operation Type	Registered Stations	Active Sites	Number of Operations
2022–2025	Smoke generator	10	9	33
	Rocket	2	1	11
Total		12	10	44

Note: This dataset only records operation frequency and site locations and lacks observed in situ precipitation increment after each seeding event. In addition, detailed year-by-year and seasonal records of precipitation seeding operations, together with precise operation boundaries, are confidential meteorological operational data and cannot be publicly released. Only the total of 44 events from 2022 to 2025 is reported in this study. The mapped coordinates refer to the locations of operation sites only and do not delineate the spatial extent of precipitation enhancement or the areas receiving additional precipitation from individual events; the county-wide grassland analysis area is the spatial domain of the ecological assessment, not an area demonstrated to have been affected by the operations. The long-term climatic attribution is therefore not used to validate the effectiveness of precipitation seeding.

2.3. Research Methods

2.3.1. NDVI Spatiotemporal Change Analysis

NDVI serves as an indicator of vegetation growth and cover, allowing changes in grassland vegetation to be monitored across space and time [16]. The interannual difference method was used to quantify changes in grassland vegetation based on annual mean growing-season NDVI [17–19]. The calculation was performed as follows:

$$C_{ij} = NDVI_i - NDVI_j \quad (1)$$

where $NDVI_i$ and $NDVI_j$ denote the average growing-season NDVI for two successive years (i and j), respectively, while C_{ij} represents the difference between these two years. Based on this method, annual differences in growing-season NDVI were calculated separately

for consecutive years within the pre-PS (2018–2021) and PS (2022–2025) periods in Wuqia County. The annual NDVI differences were then summed within each period, using 2018 and 2022 as their respective baseline years. Accordingly, the cumulative differences were equivalent to $NDVI_{2021} - NDVI_{2018}$ and $NDVI_{2025} - NDVI_{2022}$, respectively, representing net NDVI changes relative to the initial year of each period. To assess the robustness of the NDVI improvement-area estimates, sensitivity analyses were conducted using alternative baseline years (2017–2021 and 2021–2025) and adjustments of ±10% to the original NDVI improvement threshold. The within-period comparisons (2018–2021 and 2022–2025) were retained as the primary analysis.

Considering the relatively small NDVI variations in the study area, the cumulative NDVI differences (C) were classified into seven categories: severe degradation ($C \leq -0.15$), moderate degradation ($-0.15 < C \leq -0.08$), slight degradation ($-0.08 < C \leq -0.02$), relative stability ($-0.02 < C \leq 0.02$), slight improvement ($0.02 < C \leq 0.08$), moderate improvement ($0.08 < C \leq 0.15$), and high improvement ($C > 0.15$).

2.3.2. Assessment of Changes in Grassland Ecological Indicator Trends Before and During PS

Three vegetation ecological indicators, including fractional vegetation cover (FVC), net primary productivity (NPP), and the vegetation ecological quality index (VEQI), were selected to assess changes in grassland ecological conditions in Wuqia County during 2018–2025. FVC was derived from 250 m NDVI data using the dimidiate pixel model [20]. Monthly NPP was estimated using the Carnegie-Ames-Stanford Approach (CASA) model [21], based on absorbed photosynthetically active radiation (APAR) and actual light-use efficiency (ε), which was regulated by temperature and moisture stress factors. Detailed model parameterization, data processing procedures, and sensitivity and robustness assessment scenarios are provided in Appendix A (Table A1).

The dimidiate pixel model used two endmembers derived from the 2018–2025 growing-season NDVI distribution of the grassland mask: a bare-soil endmember of −0.0289 (5th percentile) and a full-vegetation endmember of 0.2543 (95th percentile). Both endmembers were held constant across pixels and years so that the two comparison periods shared an identical radiometric basis and endmember drift cannot create spurious temporal change. FVC was calculated as $(NDVI - NDVI_{soil})/(NDVI_{veg} - NDVI_{soil})$ and constrained to the range of 0–1. The percentage-scale FVC (FVC^*, 0–100) was then obtained using Equation (2). NDVI values below or above the endmembers were set to 0 and 1 before conversion. For CASA, FPAR was obtained as the arithmetic mean of an NDVI-based estimate, using $NDVI_{min} = 0.05$, $NDVI_{max} = 0.8$, $FPAR_{min} = 0.001$, $FPAR_{max} = 0.95$, and a simple-ratio-based estimate. APAR was calculated as $0.45 \times SOL \times FPAR$, with SOL converted to MJ m^{-2} $month^{-1}$. Actual light-use efficiency was $\varepsilon = \varepsilon_{max} \times T_\varepsilon \times W_\varepsilon$, where $\varepsilon_{max} = 0.542$ g C MJ^{-1}, T_ε is the CASA temperature stress scalar with $T_{opt} = 20$ °C, and W_ε is the ratio of actual to potential evaporation from ERA5-Land, constrained to 0–1. NPP was computed at a monthly step and summed from April to September. ERA5-Land fields at 0.1° were resampled to the 250 m grid before use.

Growing-season FVC was calculated as the 4–9 monthly mean, whereas cumulative growing-season NPP was obtained by summing monthly estimates over the same period. For VEQI calculation, FVC was expressed as a percentage (0–100), while NPP was normalized to 0–100 using the pixel-specific historical maximum during 2018–2025. The two standardized indicators were combined using equal weights of 0.5 to calculate VEQI [22]. The resulting dimensionless index ranges from 0 to 100, with higher values indicating better vegetation ecological quality [20].

$$FVC^* = 100 \times FVC \quad (2)$$

$$NPP^* = 100 \times \frac{NPP}{NPP_{\text{ref}}} \tag{3}$$

$$VEQI = 0.5 \times FVC^* + 0.5 \times NPP^* \tag{4}$$

where FVC^* (%) and NPP^* (dimensionless, 0–100) are the standardized indicators, $VEQI$ is a dimensionless index ranging from 0 to 100, and NPP_{ref} represents the pixel-specific maximum growing-season NPP during 2018–2025. Standardization ensures equal weighting of FVC and NPP, while the fixed pixel-specific NPP reference provides a consistent basis for comparing the pre-PS and PS operational periods. Accordingly, VEQI reflects relative vegetation ecological quality within Wuqia County during 2018–2025 rather than an absolute measure comparable across regions or periods.

Ordinary least-squares (OLS) regression was applied separately to the pre-PS (2018–2021) and PS (2022–2025) periods to estimate trends in FVC, NPP, and VEQI. Regression was performed on annual spatial means for temporal analysis and on annual pixel-level values for spatial analysis. The 95% confidence intervals (CIs) of the regional slopes and their differences were calculated to quantify uncertainty. Slope stability was further assessed using a leave-one-year-out (LOYO) sensitivity analysis, in which each annual observation was omitted in turn and the slope differences recalculated. The trend slopes and their differences between the two periods were calculated as follows:

$$Q_i = a + bt_i \tag{5}$$

$$b = \frac{n \times \sum_{i=1}^{n}(Q_i \times t_i) - \sum_{i=1}^{n} t_i \sum_{i=1}^{n} Q_i}{n \times \sum_{i=1}^{n} t_i^2 - \left(\sum_{i=1}^{n} t_i\right)^2} \tag{6}$$

$$\Delta b = b_{\text{post}} - b_{\text{pre}} \tag{7}$$

In these equations, Q_i denotes the growing-season value of a vegetation ecological indicator (FVC, NPP, or VEQI) in year t_i, while n indicates the number of years within each study period. The parameters a and b correspond to the intercept and slope of the fitted linear regression, respectively. The slopes estimated for the pre-PS and PS periods are denoted by b_{pre} and b_{post}, respectively, with Δb expressing the difference between them. Positive and negative values of b indicate upward and downward fitted trends in the corresponding ecological indicator. When Δb is positive, the slope for the PS period exceeds that of the pre-PS period, whereas a negative Δb indicates a lower slope during the PS period. However, a positive Δb does not necessarily indicate an increasing vegetation trend, as both period-specific slopes may be negative. The absolute value of $|\Delta b|$ represents the magnitude of the difference between the slopes of the two periods.

2.3.3. Ridge Regression-Based Attribution Analysis of Climatic Drivers of Grassland NDVI Changes

To identify the climatic drivers of long-term grassland NDVI changes, pixel-wise ridge regression was applied to growing-season NDVI during 2000–2025, with PET, PRE, Solar, and TMP as predictors. Ridge regression was used to reduce multicollinearity among climatic variables [23,24]. The specific procedures were as follows:

First, grassland NDVI was specified as the response variable, with PET, PRE, Solar, and TMP included as predictors, as follows:

$$\hat{\beta}_{\text{ridge}} = \left(X^{\mathrm{T}}X + \lambda \mathrm{I}\right)^{-1} X^{\mathrm{T}} y \tag{8}$$

In this equation, $\hat{\beta}_{\text{ridge}}$ denotes the ridge regression coefficient vector, while X and y correspond to the matrix of z-score-standardized climatic predictors and the z-score-standardized NDVI vector, respectively. The regularization parameter λ [25] controls the degree of coefficient penalization, and I denotes the identity matrix. By penalizing coefficient

magnitudes, ridge regression helps stabilize coefficient estimates when climatic predictors are correlated [26,27].

The ridge parameter λ was selected independently for each pixel from 81 logarithmically spaced values ranging from 10^{-4} to 10^{4}, based on the minimum mean RMSE across internal forward-chaining folds. If the optimum reached a search boundary, the range was expanded by four orders of magnitude, up to three times. The four- and three-predictor models were tuned separately, and the intercept was estimated without penalization. All computations were performed in MATLAB R2024a (The MathWorks, Inc., Natick, MA, USA).

Second, the contribution of climatic factor i to the long-term NDVI trend was determined by combining its ridge regression coefficient with the temporal trend of its standardized time series, as follows:

$$C_i = a_i S_i \tag{9}$$

In this equation, a_i represents the ridge regression coefficient of climatic factor i, S_i denotes the trend slope of its standardized time series, and C_i represents the trend contribution of this factor to long-term NDVI changes.

Third, the estimated trend contributions were used to derive the relative contribution rate and absolute trend contribution of each climatic factor using the following equations:

$$RC_i = \frac{|C_i|}{\sum_{i=1}^{n}|C_i|} \times 100\% \tag{10}$$

$$AC_i = C_i \times S_{\mathrm{NDVI}} \tag{11}$$

In these equations, RC_i denotes the percentage share attributed to climatic factor i, with the contributions of all factors totaling 100%. At each pixel, the factor with the largest RC_i is regarded as the primary climatic driver of long-term NDVI changes. AC_i denotes the absolute trend contribution of factor i, reflecting both the direction and magnitude of its contribution to NDVI changes. Positive and negative values indicate positive and negative modeled contributions to the long-term NDVI trend, respectively, rather than independent causal effects. S_{NDVI} is the sample standard deviation of the original NDVI time series. Pixels with zero or near-zero observed NDVI trends were handled explicitly in the ratio calculations: pixels with an absolute observed trend $\leq 10^{-8}$ NDVI yr^{-1} were assigned NaN, although no pixel met this criterion among the 9942 valid grassland pixels retained for the attribution analysis, and an exactly zero denominator was treated as undefined. Absolute contributions did not require such ratios, because each standardized contribution was multiplied by the standard deviation of the original NDVI series; a zero climatic trend therefore yields a zero contribution, and no near-zero threshold was imposed.

Model validation was conducted using five-fold expanding-window forward-chaining cross-validation, with training periods ending in 2010, 2013, 2016, 2019, and 2022, each followed by a three-year validation period. Model performance was assessed using R^2, RMSE, and MAE, while additional analyses included NDVI trend decomposition, AR (1) residual diagnostics, λ sensitivity, first-difference ridge regression, and bootstrap uncertainty assessment (500 pixels, 500 replicates per pixel, and three-year residual blocks).

3. Results

3.1. Spatiotemporal Changes in Grassland NDVI Before and During Precipitation Seeding

Using 2022 as the breakpoint for routine PS operations, growing-season NDVI changes were compared between the pre-PS and PS periods in Wuqia County (Figure 2). Spatially averaged annual NDVI differences fluctuated between positive and negative values. During the pre-PS period, NDVI increased in 2018–2019 (0.0002) and 2019–2020 (0.0053), but decreased in 2020–2021 (−0.0045). During the PS period, NDVI initially declined in 2022–2023

(−0.0067), followed by increases in 2023–2024 (0.0165) and 2024–2025 (0.0133). Despite the smaller annual increment in 2025, mean growing-season NDVI continued to rise, reaching 0.1770, the highest value during the study period.

Spatially, the pre-PS period was dominated by stable grassland (79.72%), with slight degradation accounting for 8.63% and slight, moderate, and high improvement accounting for 10.99%, 0.37%, and 0.06%, respectively. Degradation was mainly concentrated in central and southern Wuqia County, whereas improvement was scattered along the study area's periphery. During the PS period, stable grassland decreased to 51.28%, while slight degradation accounted for 2.11% and severe and moderate degradation together accounted for only 0.09%. In contrast, slight, moderate, and high improvement increased to 43.07%, 3.26%, and 0.19%, respectively. Improvement was particularly pronounced in northeastern Wuqia County, whereas changes in the southwest were comparatively limited. Accordingly, the proportion of grassland exhibiting slight or greater improvement increased from 11.43% in the pre-PS period to 46.52% in the PS period, a rise of 35.09 percentage points (Table 4). Sensitivity analyses using alternative baseline definitions and NDVI improvement thresholds further supported this difference. Across all six scenarios, improvement proportions ranged from 6.24% to 13.00% during the pre-PS period and from 42.94% to 53.50% during the PS period. The consistently higher improvement proportion during the PS period indicates that the observed difference was robust to the tested variations in baseline selection and classification thresholds.

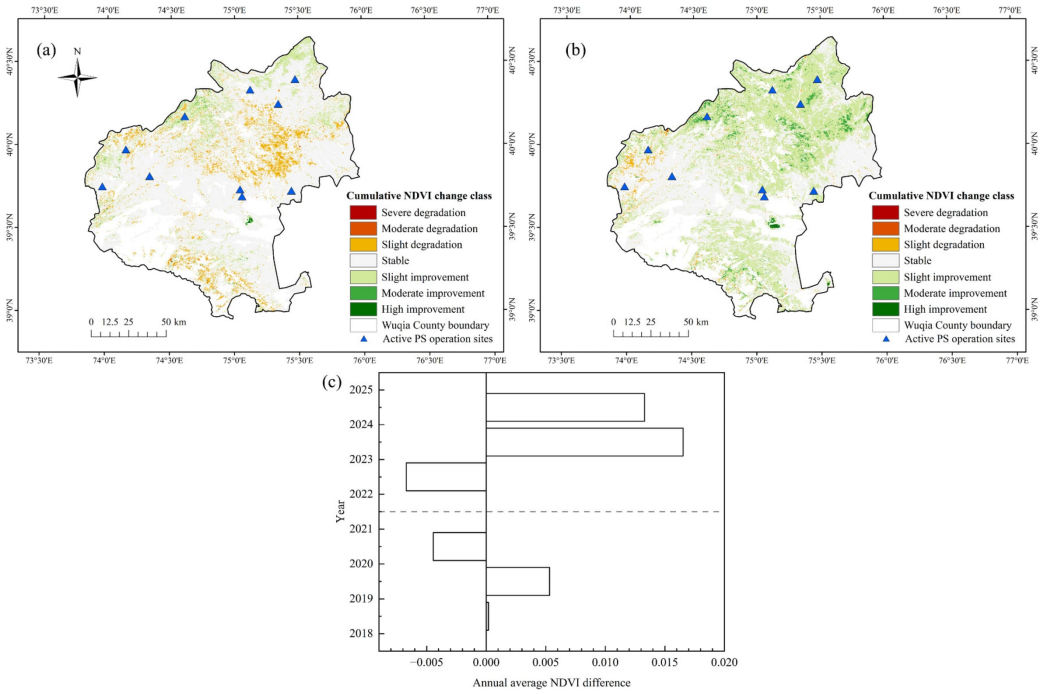


Figure 2. Spatiotemporal patterns of grassland NDVI changes in Wuqia County before (2018–2021) and during (2022–2025) precipitation seeding (PS) operations. (**a**,**b**) Cumulative growing-season NDVI changes during the two periods, respectively; (**c**) annual differences in spatially averaged growing-season NDVI within each period. The horizontal dashed line in (**c**) indicates the boundary between the pre-PS (2018–2021) and PS (2022–2025) periods, and blue triangles indicate active PS operation sites.

Table 4. Sensitivity of the proportion of grassland showing NDVI improvement to baseline selection and improvement thresholds.

Baseline Scheme	NDVI Improvement Threshold	Pre-PS (%)	PS (%)
Within-period	−10%	13.00	50.23
	Original	11.43	46.52
	+10%	10.04	42.94
Cross-period	−10%	8.28	53.50
	Original	7.17	49.94
	+10%	6.24	46.68

Note: Within-period comparisons used 2018 and 2022 as the respective baseline years for the pre-PS and PS periods. Cross-period comparisons used 2017 and 2021 as the respective baseline years for the corresponding periods (2017–2021 and 2021–2025). The original NDVI improvement threshold was 0.020, with sensitivity tests conducted using thresholds of 0.018 (−10%) and 0.022 (+10%). The '−' and '+' signs indicate decreases and increases, respectively, relative to the original NDVI improvement threshold. Improvement proportions were calculated relative to the same valid grassland analysis area across all scenarios.

3.2. Changes in Grassland Ecological Indicators Before and During Precipitation Seeding

3.2.1. Temporal Variations and Differences in Trend Slopes of Grassland Ecological Indicators

Figure 3 illustrates interannual variations in FVC, cumulative growing-season NPP, and VEQI in Wuqia County during 2018–2025. The corresponding annual spatial means are provided in Appendix A (Table A2). During 2018–2021, all three indicators increased from 2018 to 2020 before declining in 2021. During 2022–2025, they declined in 2023 and subsequently increased, reaching their highest values in 2025 (FVC: 59.1510%; NPP: 24.3658 g C m^{-2} $season^{-1}$; VEQI: 78.2728).

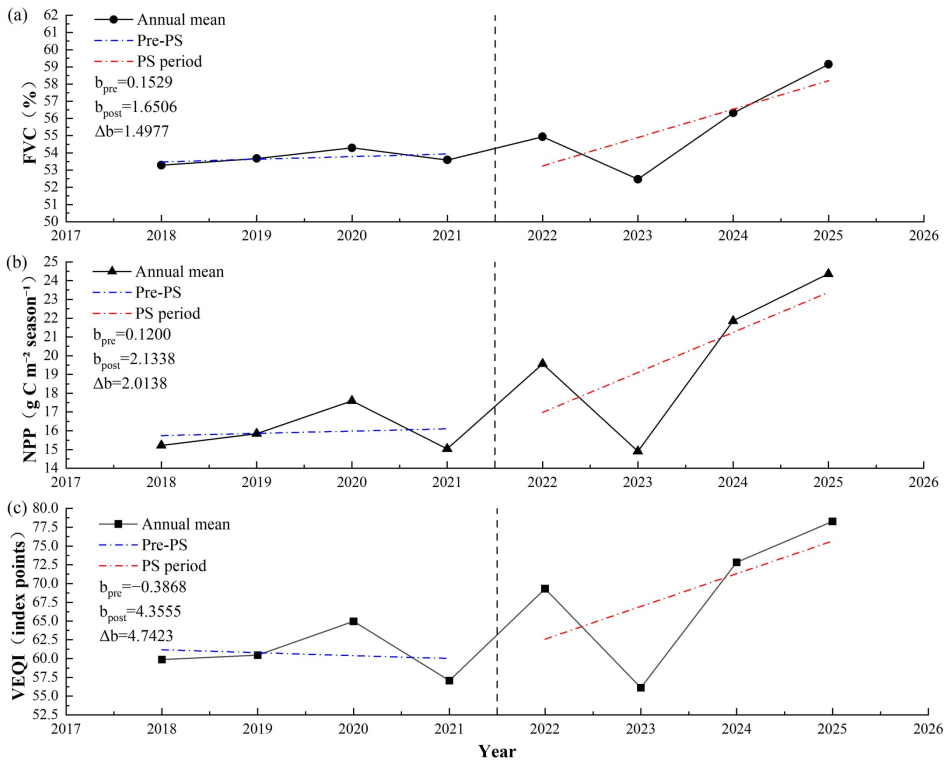


Figure 3. Interannual variations in grassland ecological indicators in Wuqia County during 2018–2025: (**a**) fractional vegetation cover (FVC, %); (**b**) cumulative growing-season net primary productivity (NPP, g C m^{-2} $season^{-1}$); and (**c**) vegetation ecological quality index (VEQI, index points). Black

symbols and lines represent annual means. Blue and red dashed lines indicate linear trends during the pre-PS (2018–2021) and PS (2022–2025) periods, respectively. The vertical dashed line separates the two periods. The corresponding trend slopes (b_{pre} and b_{post}) and their difference (Δb) are shown in each panel.

Linear regression of annual spatial means revealed higher trend slopes during the PS period than during the pre-PS period for all three indicators (Figure 3). The FVC slope increased from 0.1529 to 1.6506 percentage points yr^{-1} ($\Delta b = 1.4977$), while the NPP slope increased from 0.1200 to 2.1338 g C m^{-2} $season^{-1}$ yr^{-1} ($\Delta b = 2.0138$). Similarly, the VEQI slope increased from −0.3868 to 4.3555 index points yr^{-1} ($\Delta b = 4.7423$). Although the 95% confidence intervals of the regional Δb estimates included zero, the positive direction of the estimated changes was retained in the LOYO sensitivity analyses. Furthermore, NPP trend-slope differences remained positive across all tested FPAR, T_{opt}, and ε_{max} parameter settings (0.9909–3.0368 g C m^{-2} $season^{-1}$ yr^{-1}; Table A4). The corresponding differences in period mean values were 2.0117 percentage points for FVC, 4.2532 g C m^{-2} $season^{-1}$ for NPP, and 8.5335 index points for VEQI (PS period minus pre-PS period), providing a level-based comparison that does not depend on the number of annual observations (Table A2).

3.2.2. Spatial Patterns of Changes in Grassland Ecological Indicator Trends

Changes in the trend slopes of grassland ecological indicators exhibited pronounced spatial heterogeneity across Wuqia County (Figures 4–6; Table 2). Positive slope differences were observed across 80.48%, 85.82%, and 86.53% of the grassland area for FVC, growing-season cumulative NPP, and VEQI, respectively, indicating generally higher trend slopes during the PS period than during the pre-PS period.

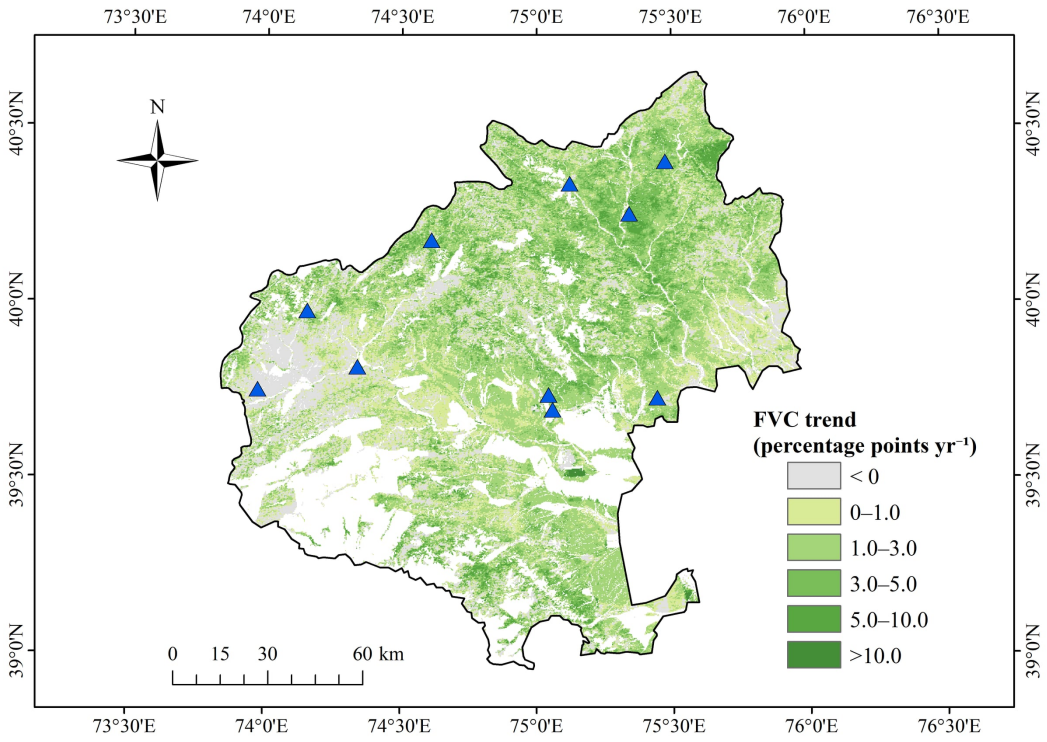


Figure 4. Spatial distribution of changes in FVC trend slopes between the pre-PS and PS periods in Wuqia County. Blue triangles indicate active PS operation sites, and white areas indicate regions outside the grassland cover. Δb denotes the difference between the PS-period and pre-PS-period trend slopes (PS minus pre-PS).

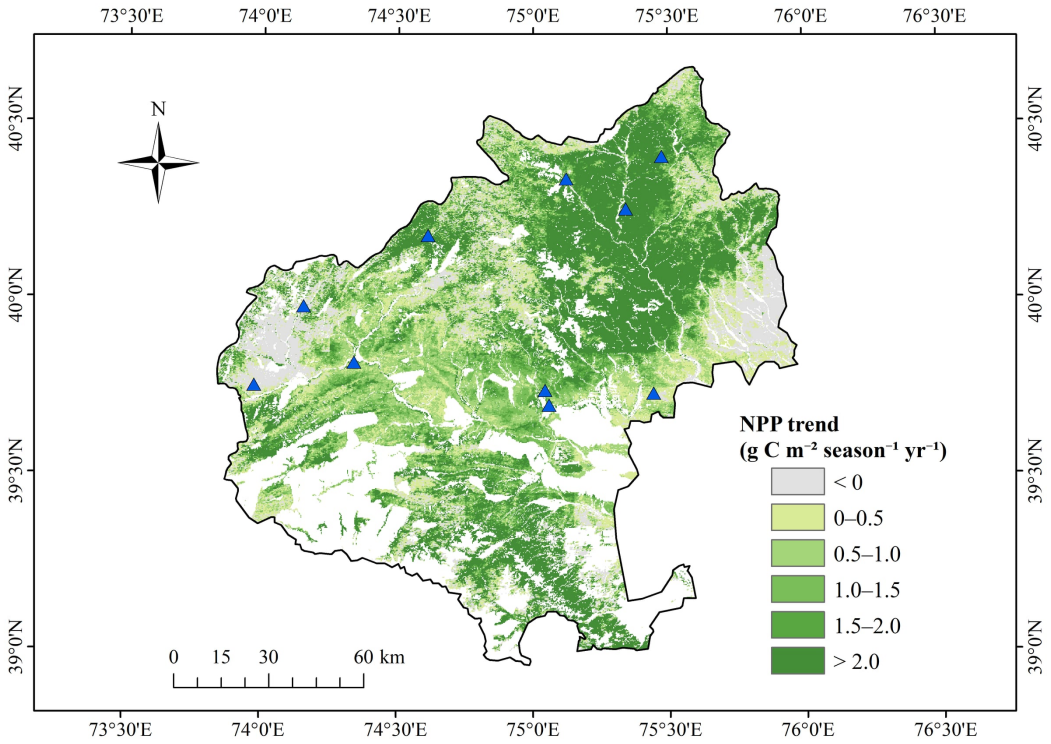


Figure 5. Spatial patterns of differences in NPP trend slopes between the pre-PS and PS periods in Wuqia County. Blue triangles indicate PS operation sites, and white areas indicate regions outside the grassland cover. Δ*b* denotes the difference between the PS-period and pre-PS-period trend slopes (PS minus pre-PS).

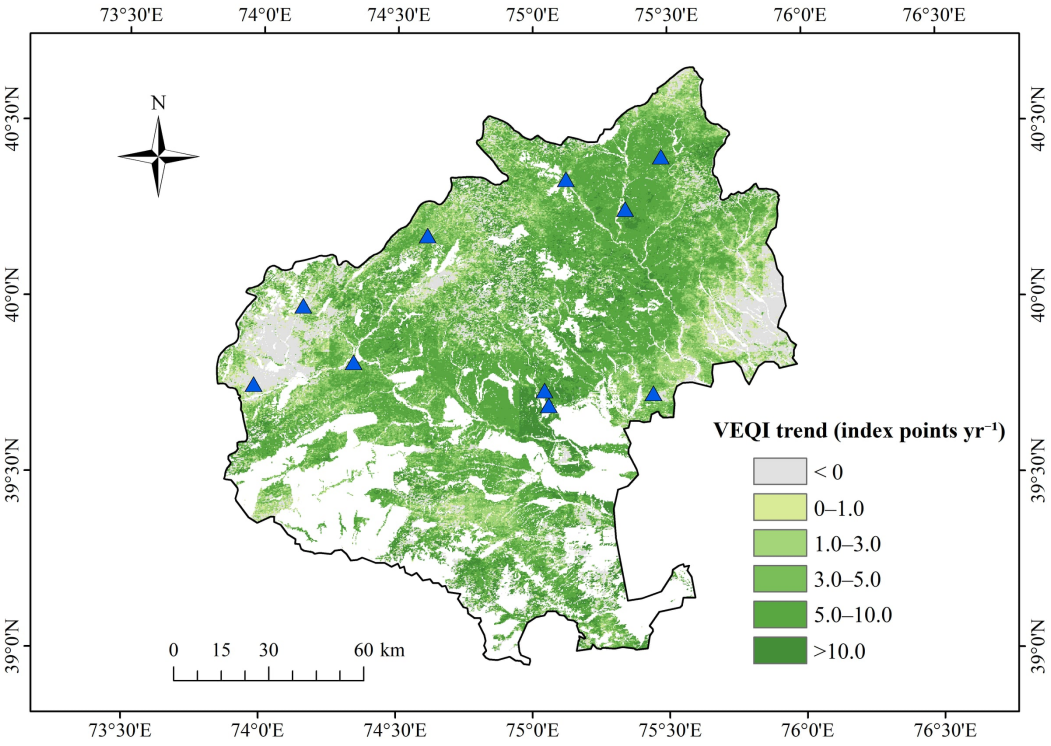


Figure 6. Spatial distribution of changes in the VEQI trend slopes between the pre-PS and PS periods in Wuqia County. Blue triangles indicate active PS operation sites, and white areas represent non-grassland land-cover types. Δ*b* denotes the difference between the PS-period and pre-PS-period trend slopes (PS minus pre-PS).

For FVC, positive slope differences were concentrated mainly in the central-eastern and northern parts of the county (Figure 4). The largest proportion (39.02%) fell within the 1–3 percentage points yr^{-1} class, followed by 0–1 (21.87%) and 3–5 percentage points yr^{-1} (15.41%). Areas with differences of 5–10 and >10 percentage points yr^{-1} accounted for 4.05% and 0.12%, respectively. Negative changes accounted for 19.52% of the grassland area and were predominantly distributed in the western region (Table 2).

For NPP, positive slope differences were widely distributed across the central, eastern, and southern regions, with larger values concentrated in the northeast and southeast (Figure 5). The largest proportion (32.93%) exhibited differences exceeding 2.0 g C m^{-2} $season^{-1}$ yr^{-1}. The remaining positive classes accounted for 14.40% (0–0.50), 16.54% (0.50–1.00), 13.11% (1.00–1.50), and 8.84% (1.50–2.00 g C m^{-2} $season^{-1}$ yr^{-1}). Negative changes affected 14.18% of the grassland area, mainly in the western region and along the eastern margins (Table 2).

For VEQI, positive trend-slope differences were widespread, accounting for 86.53% of the grassland area, while negative changes covered 13.47%. The largest proportion fell within the 5–10 index points yr^{-1} class (40.33%), followed by 3–5 (20.35%), 1–3 (14.16%), >10 (7.07%), and 0–1 (4.61%) (Figure 6; Table 2).

3.3. Climatic Drivers of Long-Term Grassland NDVI Changes

3.3.1. Relative Contributions of Climatic Factors and Their Spatial Heterogeneity

During 2000–2025, the relative contributions of individual climatic factors to long-term grassland NDVI changes varied considerably across Wuqia County (Figure 7). Among the four climatic factors, TMP had the highest mean relative contribution (55.47%), followed by potential evapotranspiration (PET, 18.35%), precipitation (PRE, 13.72%), and solar radiation (Solar, 12.46%), indicating the highest relative importance of TMP within the fitted model. The median contributions were 58.66% for TMP, 16.07% for PET, 13.58% for PRE, and 10.59% for Solar. The corresponding P10–P90 intervals were 29.99–75.37%, 3.02–36.44%, 6.17–21.11%, and 2.35–24.75%, respectively. Spatially, areas with high TMP contributions were predominantly concentrated in the northern and northeastern parts of Wuqia County. Grassland areas with TMP contributions of 40–80% accounted for 75.85% of the total grassland area, including 42.34% with contributions of 60–80%. In contrast, the proportions of grassland areas with contributions below 20% were 59.99% for PET, 85.90% for PRE, and 81.09% for Solar. Based on the dominant-factor classification at each pixel, TMP, PET, Solar, and PRE were the dominant contributors across 85.88%, 11.43%, 2.50%, and 0.19% of the grassland area, respectively. To assess the influence of PET, a three-predictor model excluding PET was fitted using the same valid pixels. TMP remained the dominant predictor, with its mean relative contribution increasing from 55.47% to 64.82% and its dominant-pixel proportion increasing from 85.88% to 92.48%. The cross-validation RMSE changed only slightly, from 0.01938 to 0.01944. These results indicate that the dominant position of TMP was robust to PET exclusion.

The probability density distributions further revealed differences in the relative contribution patterns of the four climatic factors (Figure 7e). The TMP distribution was shifted toward higher contribution levels, with a peak at 64.65%, whereas the peaks for PRE, Solar, and PET occurred at 13.20%, 4.88%, and 0.91%, respectively.

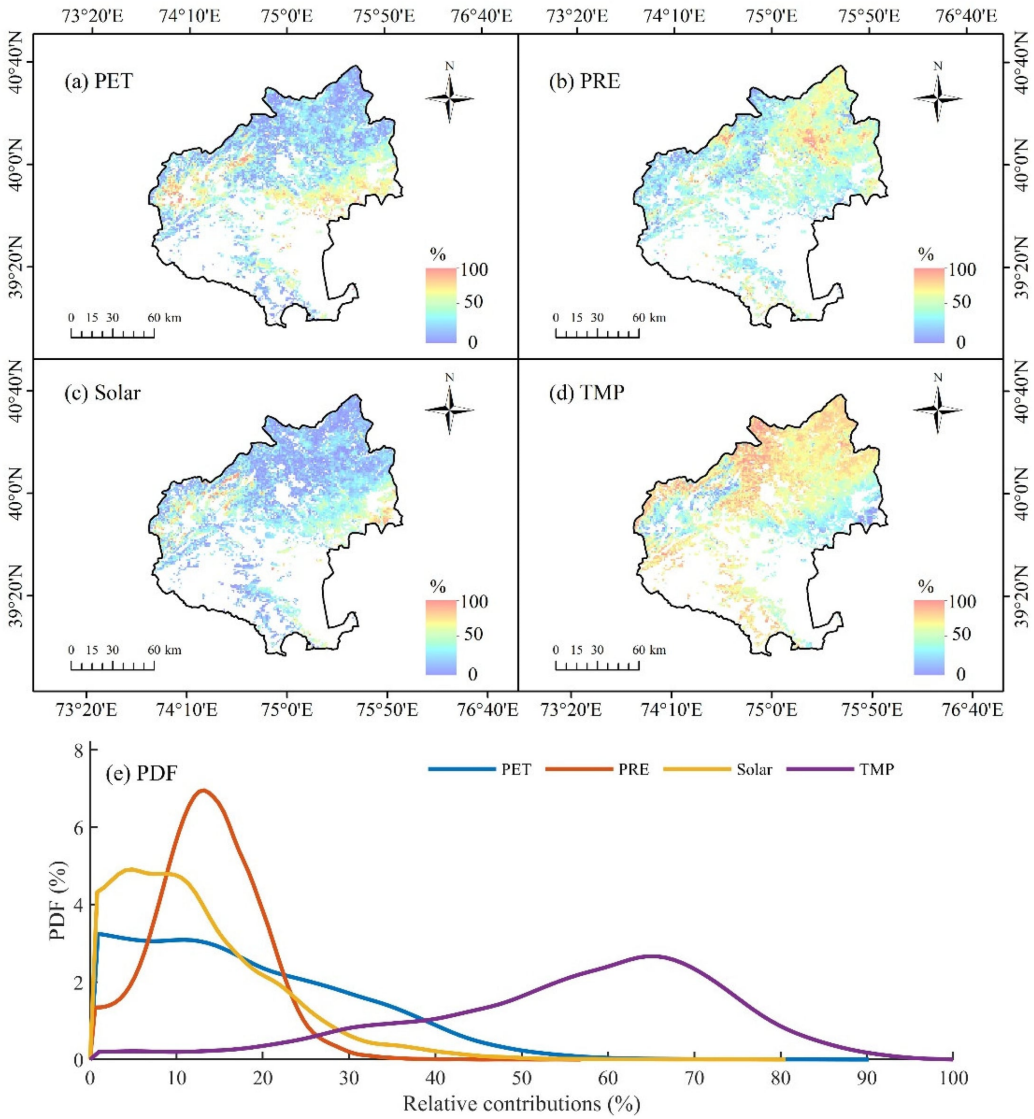


Figure 7. Spatial distribution and probability density of climatic contributions to grassland NDVI trends in Wuqia County during 2000–2025. Panels (**a**–**d**) present the relative contributions (%) of PET, PRE, Solar, and TMP, respectively, while panel (**e**) displays their probability density distributions.

3.3.2. Absolute Trend Contributions of Climatic Factors and Their Spatial Heterogeneity

Across Wuqia County, the absolute trend contributions of climatic factors to long-term grassland NDVI changes varied considerably during 2000–2025 (Figure 8). The model estimated positive mean contributions for all four climatic factors, with TMP having the largest value (0.5057×10^{-3} NDVI yr^{-1}), followed by PRE (0.1283×10^{-3} NDVI yr^{-1}), PET (0.1218×10^{-3} NDVI yr^{-1}), and Solar (0.0648×10^{-3} NDVI yr^{-1}). Spatially, positive TMP contributions occurred across 97.62% of the grassland area, with higher contributions concentrated primarily in the northern and northeastern parts of Wuqia County. PRE also showed predominantly positive contributions, covering 97.23% of the grassland area. In contrast, PET and Solar exhibited greater spatial variability, with positive contributions covering 78.39% and 79.24% of the grassland area, respectively, while negative contributions accounted for 21.61% and 20.76%, respectively (Figure 8a–d).

The probability density distributions further revealed differences in the absolute trend contributions among the four climatic factors (Figure 8e). The TMP distribution was relatively broad and shifted toward positive values, with a probability density peak at

approximately 0.210 × 10^{-3} NDVI yr^{-1}. In comparison, the peak locations for PRE, Solar, and PET were approximately 0.030, 0.015, and 0.000 × 10^{-3} NDVI yr^{-1}, respectively, indicating that their absolute trend contributions were more concentrated around zero.

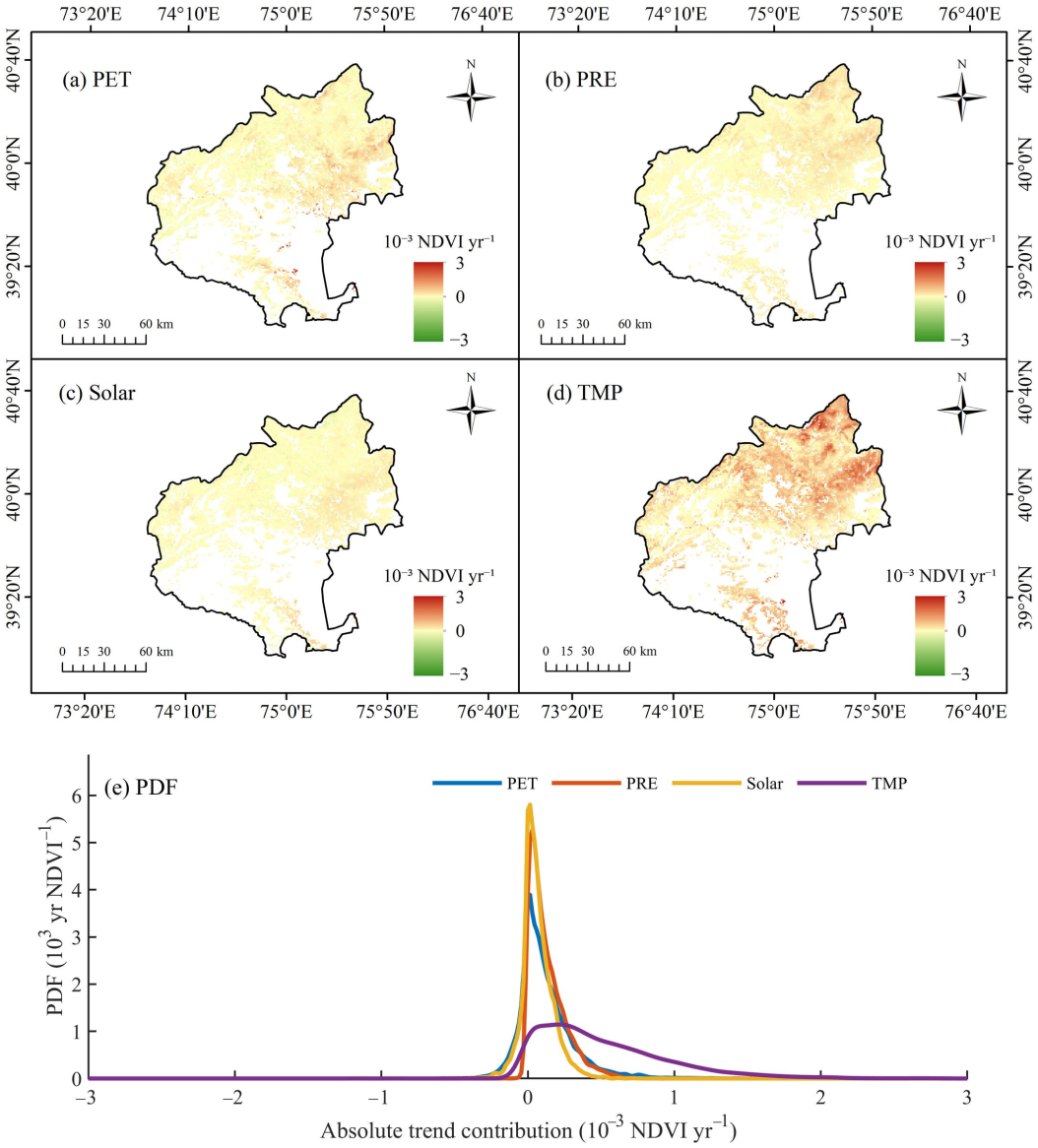


Figure 8. Spatial distributions and probability density distributions of the absolute trend contributions of climatic factors to long-term grassland NDVI changes in Wuqia County during 2000–2025. (**a**–**d**) Spatial distributions of the absolute trend contributions of PET, PRE, Solar, and TMP, respectively; (**e**) Probability density function (PDF) distributions of absolute trend contributions.

3.3.3. Model Evaluation, Robustness, and Temporal-Scale Differences in Climatic Attribution

The four-predictor model yielded a mean in-sample R^2 of 0.3934 but showed limited temporal predictive skill (mean cross-validated R^2 = −0.3986; RMSE = 0.01938; MAE = 0.01561). The observed mean NDVI trend (0.001222 NDVI yr^{-1}) was decomposed into a model-reconstructed component of 0.000821 (67.17%) and a residual component of 0.000401 (32.83%). Residuals exhibited weak positive first-order temporal autocorrelation (mean AR (1) = 0.154), while the dominant predictor remained consistent across the tested λ settings in 83.04% of valid pixels. First-difference analysis identified Solar as the leading predictor of interannual NDVI changes, accounting for 32.51% of the relative importance,

whereas TMP was the dominant long-term predictor in 85.88% of pixels (Table 5). Bootstrap analysis further supported the importance of TMP, with a median relative contribution of 48.94%, a 93.54% probability of positive contribution, and a 63.23% probability of ranking first. However, the median lower and upper bounds of pixel-level bootstrap contribution intervals were 9.85% and 86.09%, respectively, indicating substantial spatial uncertainty in TMP contribution estimates (Table A5).

Table 5. Comparison of climatic-driver importance between long-term trend attribution and first-difference analysis.

Factor	Long-Term Relative Contribution (%)	First-Difference Coefficient Importance (%)	Long-Term Dominant Pixels (%)	First-Difference Dominant Pixels (%)
PET	18.35	18.69	11.43	12.39
PRE	13.72	21.76	0.19	17.39
Solar	12.46	32.51	2.50	42.17
TMP	55.47	27.04	85.88	28.04

Note: Long-term relative contributions represent the normalized absolute trend contributions of the four climatic predictors, whereas first-difference coefficient importance represents the normalized absolute standardized coefficients of the first-difference ridge regression model. The two metrics characterize different temporal relationships and should not be interpreted as equivalent measures of explained variance. All statistics reported in this table were calculated from the valid grassland pixels that constitute the analysis area; pixels with incomplete 26-year records for the four predictors were excluded.

4. Discussion

4.1. Temporal Differences in Grassland Ecological Changes Before and During Precipitation Seeding and Their Influencing Factors

In this observational comparison, a larger proportion of grassland exhibited positive net NDVI changes during 2022–2025 than during 2018–2021, while the estimated slopes of FVC, NPP, and VEQI were higher in the operational period. These differences describe changes between the two periods and do not identify an independent effect of PS. Because FVC is derived from NDVI, CASA-based NPP uses NDVI-derived FPAR, and VEQI combines the two, agreement among the three indicators reflects shared inputs rather than independent validation. Zhou et al. [28], using MODIS NDVI data from 2008 to 2022, reported an overall increasing trend in grassland NDVI in Wuqia County, although vegetation cover remained relatively low. Their findings also suggested that grassland recovery was influenced by both climate variability and human activities. Liu et al. [29] reported that FVC and NPP generally increased across Central Asian grasslands, whereas LAI and VOD exhibited declining trends, suggesting that different vegetation indicators do not necessarily exhibit consistent temporal changes. Similarly, Xu et al. [30] integrated vegetation cover, NPP, and an ecological quality index to evaluate ecological restoration associated with PS in northwestern China. Together, these studies highlight the value of integrating multiple ecological indicators to assess grassland changes in terms of vegetation cover, productivity, and overall ecological quality.

Water availability is an important factor influencing grassland growth in arid regions, although vegetation responses to changes in water supply depend on antecedent moisture conditions, vegetation types, and environmental characteristics. Wang et al. [31], through a simulated precipitation experiment in a desert steppe, found that a 100% increase in precipitation promoted aboveground biomass accumulation during dry years. In a precipitation-gradient experiment conducted in an alpine meadow, Zhang et al. [32] observed that aboveground net primary productivity responded differently to precipitation

across years, with a nonlinear response occurring in one experimental year. This suggests that grassland productivity responses to additional water input may depend on the extent of water limitation and site-specific environmental conditions. In the present study, grassland improvements were mainly concentrated in northeastern Wuqia County, potentially reflecting spatial differences in local hydrothermal conditions, topography, and grassland management practices. However, the relationships between these factors and the spatial distribution of PS operations require further investigation.

Furthermore, the implementation of the grazing exclusion and grassland restoration program in Wuqia County since 2013 suggests that long-term ecological conservation measures may also have influenced regional grassland changes [28]. Given the spatially limited nature of PS operations and the short comparison periods, the observed differences may reflect the combined influences of natural climate fluctuations and other human activities.

4.2. Climatic Drivers of Long-Term Grassland NDVI Changes and Potential Hydrothermal Mechanisms

The four-predictor model assigned TMP the largest mean relative contribution (55.47%) to long-term grassland NDVI trends in Wuqia County during 2000–2025, with positive trend contributions across 97.62% of the grassland area. Although water availability constrains vegetation growth in arid regions, low temperatures at high elevations may also impose substantial thermal limitations. According to Ren et al. [33], rising spring temperatures facilitated vegetation growth across steppes, forests, and meadows on the northern slopes of the Tianshan Mountains, partly through increased snowmelt. In contrast, warming in other seasons may intensify drought stress and thereby suppress vegetation growth. Similarly, Zheng et al. [1] highlighted the growing influence of rising temperatures on alpine pasture greening in Central Asia, suggesting that improved thermal conditions and additional water released from melting snow and ice may jointly favor vegetation development. Cao et al. [34] found that vegetation greening in northern China's temperate grasslands was primarily driven by increased precipitation, whereas rising temperatures played a more prominent role in alpine grasslands. These findings suggest that vegetation growth in arid, high-elevation regions may be jointly regulated by thermal and moisture conditions. Moderate warming may alleviate low-temperature constraints and promote snow and ice melt, thereby improving conditions for vegetation growth. However, continued warming may also increase evaporative demand and exacerbate water stress [35]. Thus, the relatively high modeled contribution of TMP may reflect thermal limitations at high elevations, although the association also depends on water availability. Importantly, the estimated contributions represent the relative importance of climatic factors in long-term NDVI trends rather than direct measures of vegetation sensitivity or independent causal effects.

Climatic contributions also exhibited pronounced spatial heterogeneity, with TMP and PRE contributing positively across most grassland areas, whereas PET and Solar showed negative contributions in some regions. These patterns may reflect variations in hydrothermal limitations across elevation and topographic gradients. Vegetation in colder, high-elevation areas may be more strongly constrained by low temperatures, whereas relatively warm and dry areas may experience greater water limitations [36]. Under insufficient water supply, increased evaporative demand may offset the potential benefits of warming for vegetation growth [37]. Nevertheless, negative trend contributions for PET and Solar are model-derived statistical outputs for long-term NDVI trends and do not directly prove that rising PET or solar radiation suppresses vegetation growth. From the perspective of the ecological application of PS, spatial differences in hydrothermal constraints suggest that additional water inputs may generate stronger potential ecological responses in areas experiencing substantial water limitations but relatively favorable thermal conditions. Because

soil moisture, snow cover, and snow and glacier meltwater were not explicitly included in the attribution model, the direct thermal effects of temperature could not be separated from its indirect hydrological effects.

4.3. Limitations and Future Perspectives

This study has several limitations. First, FVC, NPP, and VEQI were derived from remote sensing products without independent field validation, and, as noted in Section 4.1, they share input information. Therefore, their agreement does not constitute independent validation. The sensitivity analysis assesses parameter-related uncertainty rather than model accuracy.

Second, the comparison between the pre-PS (2018–2021) and operational (2022–2025) periods was based on two short four-year windows. Each period-specific slope was estimated from only four annual values, so the slopes have very limited degrees of freedom, no reliable significance test can be attached to the difference between them, and a single anomalous year can strongly influence the fitted value. A positive slope difference therefore indicates a difference between two short-term fitted trends rather than an acceleration of an increasing trend. For this reason, differences in period mean values are also reported in Section 3.2.1 as a level-based comparison, although these differences remain sensitive to individual years. Moreover, confidential operational records and the lack of event-specific precipitation measurements prevented quantification of actual additional water input and its spatial extent. Consequently, the observed ecological changes cannot be attributed solely to PS. Natural climate variability and grazing exclusion may also have contributed.

Third, the climatic attribution results represent relative contributions to long-term NDVI trends rather than independent causal effects. Although TMP remained the dominant predictor in the PET-exclusion analysis, shared information among predictors and the omission of soil moisture, snow cover, and snowmelt limit the interpretation of climatic influences. Future research should combine integrated field monitoring of grassland communities and topsoil moisture with remote sensing observations to calibrate ecological indicators. A paired control-area design combined with measured precipitation increment from cloud-seeding events would help better isolate the net ecological effect of PS. Spatial datasets of grazing intensity should also be incorporated to decouple the ecological impacts of grazing management from the effects of precipitation seeding. Longer time-series observations would further reduce interference from interannual climate noise and improve the robustness of such assessments.

5. Conclusions

Grassland ecological conditions in Wuqia County exhibited distinct differences between the periods before (2018–2021) and during (2022–2025) precipitation seeding (PS) operations. The proportion of grassland showing slight or greater NDVI improvement increased from 11.43% to 46.52%, a difference of 35.09 percentage points, with improvements concentrated primarily in northeastern Wuqia County. FVC, cumulative growing-season NPP, and VEQI exhibited higher estimated trend slopes during the PS operational period, with positive slope differences covering 80.48%, 85.82%, and 86.53% of the grassland area, respectively. These positive slope differences indicate higher estimated slopes during the operational period rather than necessarily increasing vegetation trends. Regarding long-term climatic drivers, the four-predictor ridge regression model assigned temperature the largest mean relative share (55.47%) of modeled NDVI trend contributions during 2000–2025, with positive absolute contributions across 97.62% of the grassland area. However, temporal cross-validation revealed limited predictive performance (mean $R^2 = -0.3986$), while bootstrap analysis indicated uncertainty in the temperature ranking (63.23% probability

of ranking first). Thus, these climatic contributions should be interpreted as model-based associations rather than independent causal effects. Moreover, the observed ecological differences between the two periods cannot be attributed solely to PS because of natural climatic variability, concurrent conservation measures, the short comparison periods, and the absence of event-specific precipitation measurements and independent field validation. These findings provide an observational basis for understanding grassland ecological dynamics and their climatic associations in arid, high-elevation regions, while highlighting the need for further field monitoring and controlled assessments to evaluate the ecological effects of PS.

Author Contributions: Conceptualization, C.G. and B.B.; methodology, C.G. and B.B.; study-area boundary correction and technical guidance, Z.Z.; validation, C.C. and A.K.; formal analysis, C.G.; investigation, A.S., A.A., A.K. and C.G.; data curation, C.G., A.S. and X.Z.; writing—original draft preparation, C.G.; writing—review and editing, A.A.; visualization, C.G. and X.Z.; supervision, B.B.; funding acquisition, B.B. All authors have read and agreed to the published version of the manuscript.

Funding: This research was funded by the Natural Science Foundation of Xinjiang Uygur Autonomous Region (grant number 2026D01A88), the Open Project of Xinjiang Key Laboratory of Soil and Plant Ecological Processes (grant numbers 25XJTRZW29 and 25XJTRZW19), and the Tianshan Talent Project (grant number 2023TSYCJC0068).

Data Availability Statement: The MODIS vegetation index data were obtained from NASA Earthdata: https://www.earthdata.nasa.gov/ (accessed on 6 January 2026). Potential evapotranspiration and solar radiation data were also obtained from NASA Earthdata: https://www.earthdata.nasa.gov/ (accessed on 25 April 2026 and 27 April 2026, respectively). Monthly temperature and precipitation data for China at a spatial resolution of 1 km were sourced from the National Tibetan Plateau Data Center: https://data.tpdc.ac.cn/ (accessed on 20 April 2026).Records of precipitation seeding (PS) operations were supplied by the Meteorological Bureau of Kizilsu Kirgiz Autonomous Prefecture and the Wuqia County Meteorological Bureau.Access to these operational records is restricted under relevant data management regulations and requires authorization from the responsible meteorological authorities. The calculation code and the derived annual FVC, NPP, and VEQI rasters, together with other processed data and analysis results, are available from the corresponding author upon reasonable request.

Acknowledgments: The authors gratefully acknowledge the Meteorological Bureau of Kizilsu Kirgiz Autonomous Prefecture and the Wuqia County Meteorological Bureau for providing precipitation seeding (PS) operation records and relevant meteorological data, as well as technical support during data collection. During manuscript preparation, AI tools were used to assist with manuscript drafting, English language editing, code development, and figure layout refinement. All AI-assisted content was carefully reviewed, revised, and verified by the authors. The authors take full responsibility for the scientific analyses, interpretations, accuracy, and content of this manuscript. This study was supported by the Xinjiang Key Laboratory of Soil and Plant Ecological Processes.

Conflicts of Interest: The authors declare no conflicts of interest.

Abbreviations

The following abbreviations are used in this manuscript:

PS	Precipitation seeding
NDVI	Normalized Difference Vegetation Index
FVC	Fractional Vegetation Cover
NPP	Net Primary Productivity
VEQI	Vegetation Ecological Quality Index
PET	Potential Evapotranspiration
PRE	Precipitation
TMP	Mean Air Temperature
MODIS	Moderate Resolution Imaging Spectroradiometer

Appendix A

Table A1. FVC and CASA-NPP model parameterization, sensitivity analysis, and robustness assessment.

Component	Parameter/ Indicator	Baseline Setting or Calculation	Sensitivity Scenarios
FVC	Bare-soil NDVI	−0.0289 (5th percentile)	Fixed during 2018–2025
	Full-vegetation NDVI	0.2543 (95th percentile)	Fixed during 2018–2025
	Calculation	Dimidiate pixel model; initial FVC constrained to 0–1 and subsequently converted to percentage (0–100) by multiplying by 100	Initial FVC constrained to 0–1; percentage conversion consistently applied for subsequent analyses
FPAR	NDVI input	MOD13Q1 V6.1; QA = 0 and 1 retained; monthly mean of quality-filtered observations for CASA	Consistent NDVI input across scenarios
	Input bounds	$NDVI_{min} = 0.05$, $NDVI_{max} = 0.8$, $FPAR_{min} = 0.001$, $FPAR_{max} = 0.95$	Bounds consistently applied across scenarios
	Estimation method	MEAN: arithmetic mean of NDVI-based and SR-based FPAR estimates	NDVI-based, SR-based, and MEAN methods
APAR	Calculation	$0.45 \times SOL \times FPAR$, with SOL converted to MJ m^{-2} $month^{-1}$	Calculated under alternative FPAR methods
Light-use efficiency	Maximum light-use efficiency (ε_{max})	0.5420 g C MJ^{-1}	Baseline and ±20% scenarios (0.4336 and 0.6504 g C MJ^{-1})
Temperature stress	Optimum temperature (T_{opt})	20 °C	15, 20, and 25 °C
	Temperature stress (T_{ε})	CASA temperature stress scalar (0–1), evaluated at T_{opt} = 20 °C; applied as a multiplier in $\varepsilon = \varepsilon_{max} \times T_{\varepsilon} \times W_{\varepsilon}$ (Section 2.3.2)	Evaluated under alternative T_{opt} settings
Moisture stress	Moisture stress (W_{ε})	Ratio of absolute actual to potential evaporation from ERA5-Land, constrained to 0–1	Baseline moisture-stress formulation retained
NPP	Monthly NPP	$NPP = APAR \times \varepsilon$, with $\varepsilon = \varepsilon_{max} \times T_{\varepsilon} \times W_{\varepsilon}$; unit: g C m^{-2} $month^{-1}$	Recalculated under alternative FPAR, T_{opt}, and ε_{max} scenarios
Seasonal aggregation	Growing-season NPP	Sum of monthly NPP from April to September; unit: g C m^{-2} $season^{-1}$	Compared across parameter scenarios
Spatial matching	Meteorological inputs	ERA5-Land monthly data resampled from the native 0.1° grid to the nominal 250 m NPP output grid	Consistent output grid across scenarios
NPP uncertainty	Annual spatial mean	Baseline and alternative parameter scenarios	Comparison of annual NPP ranges and relative variations
NPP robustness	Temporal trends	OLS slopes for 2018–2021 and 2022–2025	Comparison of slopes and slope differences
NPP robustness	Spatial trends	Pixel-level slope differences between the two periods	Comparison of positive and negative change proportions

Table A1. *Cont.*

Component	Parameter/ Indicator	Baseline Setting or Calculation	Sensitivity Scenarios
VEQI robustness	Index calculation	*FVC**: FVC expressed as a percentage (0–100); *NPP**: NPP normalized to 0–100 using the pixel-specific maximum during 2018–2025; *VEQI* = 0.5 × *FVC** + 0.5 × *NPP**, with a theoretical range of 0–100.	Comparison under alternative NPP scenarios
	Alternative NPP scenarios	VEQI recalculated using alternative NPP scenarios	Comparison of *VEQI* values and trend estimates

Notes: QA = quality assurance; SR = simple ratio; FPAR = fraction of absorbed photosynthetically active radiation; APAR = absorbed photosynthetically active radiation; SOL = downward shortwave radiation; OLS = ordinary least squares.

Table A2. Annual spatial means of growing-season FVC, NPP, and VEQI in Wuqia County during 2018–2025.

Year	FVC (%)	NPP (g C m^{-2} $Season^{-1}$)	VEQI (Index Points)
2018	53.2833	15.2185	59.8721
2019	53.6711	15.8438	60.4625
2020	54.2929	17.5925	64.9766
2021	53.5858	15.0355	57.0780
2022	54.9326	19.5701	69.3203
2023	52.4726	14.9081	56.1164
2024	56.3237	21.8593	72.8136
2025	59.1510	24.3658	78.2728

Note: Annual spatial means were calculated separately for each indicator and year. NPP is reported as the cumulative growing-season total (g C m^{-2} $season^{-1}$).

Table A3. Summary statistics of trend-slope differences, regional trend estimates, and leave-one-year-out sensitivity results for FVC, NPP, and VEQI in Wuqia County.

Indicator	FVC (Percentage Points yr^{-1})	NPP (g C m^{-2} $Season^{-1}$ yr^{-1})	VEQI (Index Points yr^{-1})
Mean	1.4977	2.0138	4.7423
Minimum	−19.7964	−27.2674	−14.1634
Maximum	26.7541	45.8120	24.0815
SD	1.9819	2.5441	3.2842
Pre-PS slope (95% CI)	0.1529 (−0.7307, 1.0366)	0.1200 (−2.6031, 2.8431)	−0.3868 (−8.0063, 7.2326)
PS slope (95% CI)	1.6506 (−2.5824, 5.8837)	2.1338 (−4.7692, 9.0368)	4.3555 (−13.4732, 22.1842)
Δ*b* (95% CI)	1.4977 (−2.5113, 5.5067)	2.0138 (−3.9728, 8.0005)	4.7423 (−10.5179, 20.0024)
LOYO minimum Δ*b*	0.5427	0.9468	1.8032
LOYO maximum Δ*b*	3.1863	4.6088	11.4650
Δ*b* with 2023 omitted	1.1517	1.4137	3.1942

Note: Trend-slope differences were calculated as the PS-period slope (2022–2025) minus the pre-PS-period slope (2018–2021). Regional slopes were estimated using OLS regression of annual spatial means. Values in parentheses indicate 95% confidence intervals. LOYO denotes leave-one-year-out sensitivity analysis. The LOYO minimum and maximum represent the range of slope differences obtained by omitting one year at a time, rather than confidence intervals. FVC is expressed as a percentage (0–100), so its slope and slope difference are reported in percentage points yr^{-1}; on a 0–1 fractional scale the same slope difference corresponds to approximately 0.0150. NPP trend-slope differences are expressed in g C m^{-2} $season^{-1}$ yr^{-1}.

Table A4. Sensitivity of CASA-derived NPP to alternative parameter settings and their effects on temporal trends.

Sensitivity Test	Scenario	Parameter Setting	NPP (g C m^{-2} $Season^{-1}$)	Relative Change (%)	Pre-PS Slope (g C m^{-2} $Season^{-1}$ yr^{-1})	PS Slope (g C M^{-2} $Season^{-1}$ yr^{-1})	Δb (g C m^{-2} $Season^{-1}$ yr^{-1})
FPAR	NDVI	NDVI-based	28.5380	+58.11	0.1783	3.2151	3.0368
FPAR	MEAN	MEAN	18.0492	0.0000	0.1200	2.1338	2.0138
FPAR	SR	SR-based	7.5604	−58.11	0.0616	1.0525	0.9909
T_{opt}	Low	15 °C	25.9283	+43.65	0.2508	2.6607	2.4099
T_{opt}	Baseline	20 °C	18.0492	0.0000	0.1200	2.1338	2.0138
T_{opt}	High	25 °C	10.1639	−43.69	0.0331	1.3522	1.3191
ε_{max}	Low	0.4336 (−20%)	14.4394	−20.00	0.0960	1.7071	1.6111
ε_{max}	Baseline	0.5420	18.0492	0.0000	0.1200	2.1338	2.0138
ε_{max}	High	0.6504 (+20%)	21.6590	+20.00	0.1440	2.5606	2.4166

Note: Δb represents the difference between the PS and pre-PS slopes. Relative changes are calculated against the corresponding baseline parameter setting. In the Relative Change (%) column, '+' and '−' indicate increases and decreases in NPP, respectively, relative to the corresponding baseline parameter setting. Sensitivity ranges indicate parameter-induced uncertainty rather than model prediction errors.

Table A5. Summary of model performance, NDVI trend decomposition, residual diagnostics, and robustness assessments of the four-predictor climatic attribution model.

Assessment	Metric	Result
Model performance	Mean in-sample R^2	0.3934
	Mean cross-validated R^2	−0.3986
	Mean cross-validated RMSE	0.0194
	Mean cross-validated MAE	0.0156
NDVI trend decomposition	Observed NDVI trend (NDVI yr^{-1})	0.0012
	Reconstructed trend (NDVI yr^{-1})	0.0008
	Reconstructed contribution (%)	67.1700
	Residual trend (NDVI yr^{-1})	0.0004
	Residual contribution (%)	32.8300
Residual diagnostics	Mean AR (1) coefficient	0.1540
λ robustness	Dominant-predictor consistency across λ settings (%)	83.0400
Bootstrap assessment	Median relative contribution of TMP (%)	48.9400
	Positive-contribution probability (%)	93.5400
	Probability of TMP ranking first (%)	63.2300
	Median lower endpoint of pixel-level contribution intervals (%)	9.8500
	Median upper endpoint of pixel-level contribution intervals (%)	86.0900

Note: R^2 = coefficient of determination; RMSE = root mean square error; MAE = mean absolute error; AR (1) = first-order autocorrelation coefficient; λ = ridge regression penalty parameter; TMP = mean air temperature. The lower and upper endpoints represent the median values of the corresponding pixel-level bootstrap contribution intervals.

Table A6. Sensitivity of climatic-driver attribution to the exclusion of PET.

Comparison Metric	Four-Predictor Model	Three-Predictor Model (PET Excluded)
TMP relative contribution (%)	55.4700	64.8200
Pixels dominated by TMP (%)	85.8800	92.4800
Mean cross-validated RMSE	0.0194	0.0194

Note: TMP = mean air temperature; RMSE = root mean square error. Relative contributions were normalized separately within each model.

References

1. Zheng, L.; Xu, J.; Li, D.; Xia, Z.; Chen, Y.; Xu, G.; Lu, D. Increasing control of climate warming on the greening of alpine pastures in central Asia. *Int. J. Appl. Earth Obs. Geoinf.* **2021**, *105*, 102606. [CrossRef]
2. Zhou, Y.; Li, Y.; Li, W.; Li, F.; Xin, Q. Ecological Responses to Climate Change and Human Activities in the Arid and Semi-Arid Regions of Xinjiang in China. *Remote Sens.* **2022**, *14*, 3911. [CrossRef]
3. Kim, B.-Y.; Cha, J.W.; Jung, W.; Ko, A.R. Precipitation Enhancement Experiments in Catchment Areas of Dams: Evaluation of Water Resource Augmentation and Economic Benefits. *Remote Sens.* **2020**, *12*, 3730. [CrossRef]
4. U.S. Government Accountability Office. *Cloud Seeding Technology: Assessing Effectiveness and Other Challenges*; GAO-25-107328; U.S. Government Accountability Office: Washington, DC, USA, 2024. Available online: https://www.gao.gov/products/gao-25-107328 (accessed on 15 January 2026).
5. Wang, W.; Zhang, M.; Ma, L. Evaluation of Aircraft Cloud Seeding for Ecological Restoration in the Shiyang River Basin Using Remote Sensing. *Atmosphere* **2025**, *16*, 1344. [CrossRef]
6. Ma, L.; Wang, W.; Fan, H.; Li, Y. Validation and Assessment of Artificial Rainfall Enhancement Effects in Shiyang River Basin using Google Earth Engine Data. *Desert Oasis Meteorol.* **2025**, *19*, 182–190. [CrossRef]
7. Gong, Y.; Liu, X.; Wu, X.; Wang, C.; Han, J.; Deng, W.; Pan, X. Evaluation of Ecological Effect of Artificial Precipitation Enhancement in Daxinganling Range Based on Remote Sensing. *Desert Oasis Meteorol.* **2026**, *20*, 51–58.
8. Zhang, C.; Yao, H.; Ma, X. Spatiotemporal Dynamics and Attribution Analysis of Net Ecosystem Productivity in the Tianshan Region. *Ecol. Environ. Sci.* **2025**, *34*, 1690–1704. [CrossRef]
9. Wang, L.; Fang, W.; Lu, J.; Liu, Z. A study on tectonic geomorphology and landscape ecological pattern in the Kangsu area, Wuqia, Xinjiang. *J. Geomech.* **2022**, *28*, 101–112. [CrossRef]
10. Xun, Q.; An, S.; Lu, M. Climate change and topographic differences influence grassland vegetation greening across environmental gradients. *Front. Environ. Sci.* **2024**, *11*, 1324742. [CrossRef]
11. Lu, J.; Fang, W.; Wang, L.; Liu, Z.; Hao, G. Relationship between land use status, soil type and ecological environment resources of Wuqia in Xinjiang. *J. Guilin Univ. Technol.* **2020**, *40*, 323–329. [CrossRef]
12. Wuqia County People's Government; Wuqia County Agriculture and Rural Affairs Bureau. *Implementation Plan for the 2025 Grassland Ecological Protection Subsidy and Reward Policy in Wuqia County*; Wuqia County People's Government Website: Wuqia, China, 2025.
13. Rui, H.; Luo, B.; Wang, Y.; Zhu, L.; Zhu, Q. Quantitative impacts of climate change and human activities on grassland growth in Xinjiang, China. *Front. Plant Sci.* **2025**, *15*, 1497248. [CrossRef]
14. Chen, J.; Jönsson, P.; Tamura, M.; Gu, Z.; Matsushita, B.; Eklundh, L. A simple method for reconstructing a high-quality NDVI time-series data set based on the Savitzky–Golay filter. *Remote Sens. Environ.* **2004**, *91*, 332–344. [CrossRef]
15. Peng, S.; Ding, Y.; Liu, W.; Li, Z. 1 km monthly temperature and precipitation dataset for China from 1901 to 2017. *Earth Syst. Sci. Data* **2019**, *11*, 1931–1946. [CrossRef]
16. Tucker, C.J. Red and Photographic Infrared Linear Combinations for Monitoring Vegetation. *Remote Sens. Environ.* **1979**, *8*, 127–150. [CrossRef]
17. Han, B.; Zhou, B.; Yan, Y.; Shi, M.; Su, S.; Zhao, H.; Niu, D.; Fu, H. Analysis of Vegetation Coverage Change and Its Driving Factors over Tibetan Plateau From 2000 to 2008. *Acta Agrest. Sin.* **2019**, *27*, 1651–1658. [CrossRef]
18. Huang, X.; Zhou, Z.; Zhao, X.; Wu, G.; Long, Y.; Chen, J. Information extraction and characteristic analysis of cultivated land abandonment in karst rocky desertification mountainous areas based on time-series vegetation index. *Sci. Rep.* **2025**, *15*, 12554. [CrossRef]
19. Mancino, G.; Falciano, A.; Trivigno, M.L. Change Detection methods for forest expansion assessment in the last twenty years in the Mediterranean Basin. *iForest* **2025**, *18*, 69–78. [CrossRef]
20. China Meteorological Administration. *Grade of Monitoring and Evaluating for Terrestrial Vegetation Meteorology and Ecological Quality*; China Meteorological Administration: Beijing, China, 2019.

21. Potter, C.S.; Randerson, J.T.; Field, C.B.; Matson, P.A.; Vitousek, P.M.; Mooney, H.A.; Klooster, S.A. Terrestrial ecosystem production: A process model based on global satellite and surface data. *Glob. Biogeochem. Cycles* **1993**, *7*, 811–841. [CrossRef]
22. Zou, J.; Wang, Q.; Liu, D.; Ding, J.; Xue, Y.; Yang, L.; Ma, J. Remote Sensing-Based Assessment of Vegetation Ecological Quality and Ecological Water Requirement Thresholds in Central Asia. *Land* **2026**, *15*, 1101. [CrossRef]
23. Hoerl, A.E.; Kennard, R.W. Ridge Regression: Biased Estimation for Nonorthogonal Problems. *Technometrics* **1970**, *12*, 55–67. [CrossRef]
24. Zhao, Y.; Chen, Y.; Wu, C.; Li, G.; Ma, M.; Fan, L.; Zheng, H.; Song, L.; Tang, X. Exploring the contribution of environmental factors to evapotranspiration dynamics in the Three-River-Source region, China. *J. Hydrol.* **2023**, *626*, 130222. [CrossRef]
25. Roberts, D.R.; Bahn, V.; Ciuti, S.; Boyce, M.S.; Elith, J.; Guillera-Arroita, G.; Hauenstein, S.; Lahoz-Monfort, J.J.; Schröder, B.; Thuiller, W.; et al. Cross-validation strategies for data with temporal, spatial, hierarchical, or phylogenetic structure. *Ecography* **2017**, *40*, 913–929. [CrossRef]
26. Li, G.; Wu, C.; Chen, Y.; Huang, C.; Zhao, Y.; Wang, Y.; Ma, M.; Ding, Z.; Yu, P.; Tang, X. Increasing temperature regulates the advance of peak photosynthesis timing in the boreal ecosystem. *Sci. Total Environ.* **2023**, *882*, 163587. [CrossRef]
27. Walker, E.; Birch, J.B. Influence Measures in Ridge Regression. *Technometrics* **1988**, *30*, 221–227. [CrossRef]
28. Zhou, M.; Liang, J.; Li, G.; Yang, Z.; Chai, C. Assessment of the Contribution of the Returning Pasture to Grassland Project on Grassland Vegetation Restoration in Wuqia County. *Chin. J. Grassl.* **2025**, *47*, 13–26. [CrossRef]
29. Liu, L.; Zheng, J.; Guan, J.; Li, C.; Ma, L.; Liu, Y.; Han, W. Strong positive direct impact of soil moisture on the growth of central asian grasslands. *Sci. Total Environ.* **2024**, *954*, 176663. [CrossRef]
30. Xu, L.; Duan, J.; Zhao, Y.; Chen, Z.; Zhai, W. Separation evaluation and validation of artificial precipitation enhancement benefits on ecological restoration in the northwest China. *Acta Ecol. Sin.* **2026**, *46*, 822–831. [CrossRef]
31. Wang, Y.; Wang, Z.; Li, H.; Sun, H.; Shen, T.; Song, X.; Wang, Z.; Han, G. Simulated precipitation change drives plant diversity and biomass change in the desert steppe. *Plant Ecol. Divers.* **2022**, *15*, 127–136. [CrossRef]
32. Zhang, F.; Quan, Q.; Song, B.; Sun, J.; Chen, Y.; Zhou, Q.; Niu, S. Net primary productivity and its partitioning in response to precipitation gradient in an alpine meadow. *Sci. Rep.* **2017**, *7*, 15193. [CrossRef]
33. Ren, J.; Liu, H.; Yin, Y.; He, S. Drivers of greening trend across vertically distributed biomes in temperate arid Asia. *Geophys. Res. Lett.* **2007**, *34*, L07707. [CrossRef]
34. Cao, F.; Liu, L.; Rong, Y.; Jiang, N.; Zhao, L.; Zhang, Q.; Wu, Z.; Zhao, W.; Li, S. Climate change enhances greening while human activities accelerate degradation in northern China's grasslands. *Sci. Total Environ.* **2025**, *966*, 178570. [CrossRef]
35. Tao, J.; Wei, D.; Qi, Y.; Wang, Z.; Hua, L.; Wang, X. Soil Moisture Rather Than Atmospheric Dryness Dominates CO_2 Uptake in an Alpine Steppe. *J. Geophys. Res. Biogeosci.* **2023**, *128*, e2023JG007593. [CrossRef]
36. Wang, Y.; Peng, D.; Shen, M.; Xu, X.; Yang, X.; Huang, W.; Yu, L.; Liu, L.; Li, C.; Li, X.; et al. Contrasting Effects of Temperature and Precipitation on Vegetation Greenness along Elevation Gradients of the Tibetan Plateau. *Remote Sens.* **2020**, *12*, 2751. [CrossRef]
37. Wen, R.; Jiang, P.; Qin, M.; Jia, Q.; Cong, N.; Wang, X.; Meng, Y.; Yang, F.; Liu, B.; Zhu, M.; et al. Regulation of NDVI and ET negative responses to increased atmospheric vapor pressure deficit by water availability in global drylands. *Front. For. Glob. Change* **2023**, *6*, 1164347. [CrossRef]

Disclaimer/Publisher's Note: The statements, opinions and data contained in all publications are solely those of the individual author(s) and contributor(s) and not of MDPI and/or the editor(s). MDPI and/or the editor(s) disclaim responsibility for any injury to people or property resulting from any ideas, methods, instructions or products referred to in the content.